Robust graphene-based molecular devices

El Abbassi, Maria; Sangtarash, Sara; Liu, Xunshan; Perrin, Mickael Lucien; Braun, Oliver; Lambert, Colin; van der Zant, Herre Sjoerd Jan; Yitzchaik, Shlomo; Decurtins, Silvio; More Authors

DOI
10.1038/s41565-019-0533-8

Publication date
2019

Document Version
Final published version

Published in
Nature Nanotechnology

nature nanotechnology

LETTERS

https://doi.org/10.1038/s41565-019-0533-8

Robust graphene-based molecular devices

Maria El Abbassi[1,2,3], Sara Sangtarash[4,5], Xunshan Liu[6], Mickael Lucien Perrin[1], Oliver Braun[1,2], Colin Lambert[4], Herre Sjoerd Jan van der Zant[3], Shlomo Yitzchaik[7], Silvio Decurtins[6], Shi-Xia Liu[6*], Hatef Sadeghi[4,5*] and Michel Calame[1,2,8*]

One of the main challenges to upscale the fabrication of molecular devices is to achieve a mechanically stable device with reproducible and controllable electronic features that operates at room temperature[1,2]. This is crucial because structural and electronic fluctuations can lead to significant changes in the transport characteristics at the electrode–molecule interface[3,4]. In this study, we report on the realization of a mechanically and electronically robust graphene-based molecular junction. Robustness was achieved by separating the requirements for mechanical and electronic stability at the molecular level. Mechanical stability was obtained by anchoring molecules directly to the substrate, rather than to graphene electrodes, using a silanization reaction. Electronic stability was achieved by adjusting the π–π orbitals overlap of the conjugated head groups between neighbouring molecules. The molecular devices exhibited stable current–voltage (I–V) characteristics up to bias voltages of 2.0 V with reproducible transport features in the temperature range from 20 to 300 K.

To realize reliable graphene-based junctions, several issues exist to date and need to be addressed. First, graphene-based junctions were reported to exhibit signatures similar to those of molecules, with gate-dependent resonance features, such as Coulomb blockade[5,6], quantum interference[7] and Fabry–Perrot resonances[8]. Second, connecting molecules to the graphene remains challenging due to the lack of control on the electrode geometry at the nanoscale[4,5,8–10]. To achieve both mechanical stability and electrical reproducibility at the same time imposes different requirements on the junction properties[3,11]. Finding a proper balance between the electronic and mechanical stability is therefore challenging. Weakly coupled π–π stacking is believed to be an appealing strategy to anchor molecules to the contact electrodes[3], and offers advantages such as a high thermoelectric efficiency. However, this approach was shown to lead to mechanically unstable junctions[12]. Alternatively, molecules were also bonded covalently to graphene to yield mechanically stable junctions[10]. Unfortunately, transport through strongly coupled molecules is expected to be heavily influenced by the electrode geometry, edge termination and crystallographic structure, and lead to a large variability in the shape of the I–V characteristics[3]. Third, junction-to-junction variability remains high for the above-mentioned anchoring methods[13,14], which leads to poor device reproducibility. Finally, the silicon dioxide substrate itself was reported to yield feature-rich charge-transport characteristics[15], in particular due to switching within the oxide[16], which may be confused with molecular signatures.

The molecule we propose (Fig. 1a) contains three main parts, a silane group and a π-conjugated head group, decoupled by a non-conjugated alkane chain. The silane part is responsible for the mechanical anchoring of the molecule by forming a covalent bond with the substrate. This silanization process is commonly used to cover surfaces with organofunctional molecules[17–19]. This approach offers distinct advantages. As the graphene edges usually present ill-defined edge terminations after nanofabrication and/or the preparation of the contact electrodes, anchoring the molecules to the substrate seems a valid possible alternative. In addition, as the molecules are covalently bonded to the substrate, this process leads to mechanically stable graphene–molecule junctions. Moreover, the silanization process also passivates the silicon dioxide surface and prevents unwanted switching effects[16]. The second part of the molecule is the conjugated head group, specifically a biphenyl N-carbazole group (molecule BPC), whose orbitals can couple to the π orbitals of the graphene. The alkane chain is the final necessary element, whose crucial role is to electronically decouple the mechanical anchoring from the electronic head group. Density functional theory (DFT) calculations (Methods and Supplementary Section II) confirmed that the frontier orbitals of the BPC molecule are, indeed, solely localized on the head group. These calculations also show that head groups of two neighbouring molecules can π–π stack to form transport channels that are delocalized across all the head groups. A schematic illustration of BPC molecules assembled in the graphene nanogap with π–π-stacked head groups is shown in Fig. 1b.

To correlate the junction stability and electrical properties with the molecular structure, several test molecules with different head groups were designed and investigated. The first test molecule is methyl terminated (abbreviated as molecule M). In the absence of a delocalized π system, it is expected to only poorly conduct charges. The second test molecule possess an N-carbazole head group (abbreviated as molecule C). The π system of molecule C has two phenyl rings fewer than the BPC molecule. The lack of phenyl rings leads to a reduction in the orbital overlap by about a factor of two, which results in a lower interaction energy between neighbouring head groups[3]. Owing to its smaller interaction energy, molecule C is therefore expected to form less stable transport channels than the BPC molecule[3]. Descriptions of the device fabrication and molecule deposition are given in Methods.

Figure 1c–e presents the electrical characterization of three devices, each exposed to one of the molecules under study. For this purpose, the I–V characteristics were acquired at room temperature by averaging a back-and-forth voltage sweep. For each device, 100

[1]Empa, Swiss Federal Laboratories for Materials Science and Technology, Transport at Nanoscale Interfaces Laboratory, Dübendorf, Switzerland. [2]Department of Physics, University of Basel, Basel, Switzerland. [3]Kavli Institute of Nanoscience, Delft University of Technology, Delft, The Netherlands. [4]Department of Physics, Lancaster University, Lancaster, UK. [5]School of Engineering, University of Warwick, Coventry, UK. [6]Department of Chemistry and Biochemistry, University of Bern, Bern, Switzerland. [7]Institute of Chemistry, The Hebrew University of Jerusalem, Jerusalem, Israel. [8]Swiss Nanoscience Institute, University of Basel, Basel, Switzerland. *e-mail: liu@dcb.unibe.ch; h.sadeghi@lancaster.ac.uk; michel.calame@empa.ch

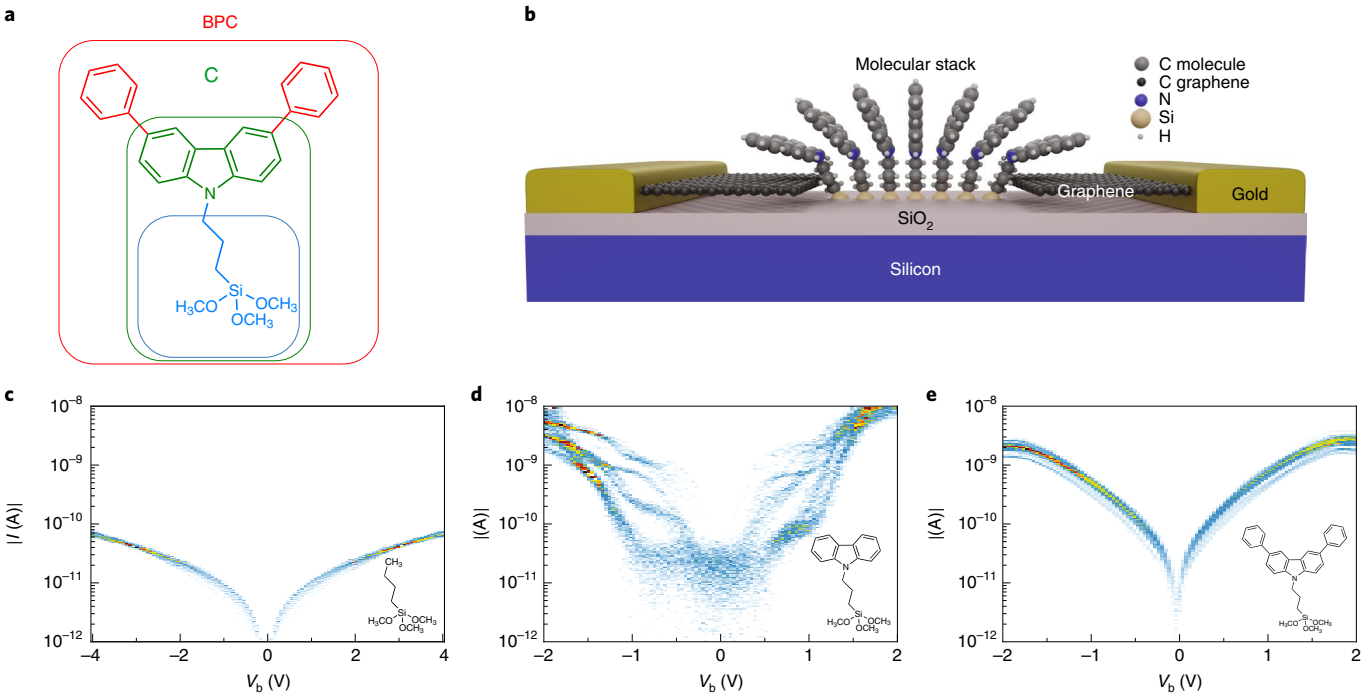

Fig. 1 | Junction geometry, molecular design and electrical characterization. a, Drawing of the three molecules, constituted of three main parts: the silane group for the covalent anchoring to the substrate, the alkane chain that decouples the silane group from the different head groups (CH_3 (molecule M) and N-carbazole (molecule C)) and biphenyl N-carbazole (molecule BPC). **b**, Schematic illustration of a molecular junction that contains a series of π–π-stacked molecules bridging a graphene nanogap. The atomic positions of the molecules are for illustrative purposes only, and do not correspond to the DFT-relaxed geometry shown in Fig. 4. For clarity, different sizes and colours are used to distinguish the carbon atoms of the molecule from those of the graphene. **c**–**e**, The electrical measurements that correspond to the three molecules under study with different head groups are displayed as density plots of the measured *I*–*V* curves, of which the absolute value of the current is plotted on a logarithmic scale. For each molecule, 100 *I*–*V* curves without data selection were measured at room temperature on a specific device per molecule.

I–*V* curves were measured and combined into a density plot without any data selection. This density plot consisted of a two-dimensional histogram of all the *I*–*V* curves recorded on the device, constructed by binning both the current and the voltage axes. For the current axis, the absolute value of the current on a log scale was used. The density plots are a colour-coded representation of such histograms, in which the areas of high counts can be identified that correspond to the most likely device behaviour. The density plots are normalized by the total number of data points.

The junction that contains molecule M (Fig. 1c) presents a single category of tunnelling-like *I*–*V* curves, with a maximum current of about 10 pA at a bias voltage (V_b) of 2 V. The *I*–*V* curves recorded on junctions exposed to molecule C are shown in Fig. 1d. The maximum currents are about two orders of magnitude larger than that for molecule M, which indicates that the π–π stacking leads to a more efficient charge transport across the molecular junction. However, the plot also exhibits large variations in the *I*–*V* shapes and current levels. These fluctuations are attributed to the weak electronic interaction between the neighbouring head groups, which allows for various molecular conformations to occur, each of them possibly with slightly different electronic properties (a more detailed study is presented in Supplementary Section III). Figure 1e shows the density plot of the *I*–*V* curves recorded for a device after the deposition of molecule BPC. Contrary to molecule C, the BPC molecule leads to both a higher current and a higher stability, as shown by the high similarity of the 100 *I*–*V* curves recorded at room temperature.

Stability and intersample reproducibility at 20 K

We performed electrical measurements at cryogenic temperatures (20 K) to spectroscopically characterize the BPC molecular junctions. Figure 2 presents an overview of these measurements, and Fig. 2a shows three individual *I*–*V* curves recorded on each device. We successively measured 100 such *I*–*V* curves. The 100 *I*–*V* curves were then used to construct density plots (Fig. 2b), as described previously. Here, only one category of *I*–*V* curves was observed, with small fluctuations. Furthermore, all the devices exhibited similar current levels (within one order of magnitude) and curve shape. The insets show the corresponding average *I*–*V* curve ($\langle I \rangle$), which exhibits a very similar shape to the individual *I*–*V* curves shown in Fig. 2a. Finally, the numerical derivative of $\langle I \rangle$ was calculated (Fig. 2c) to obtain the differential conductance ($\mathrm{d}\langle I \rangle/\mathrm{d}V$) traces (blue line). As a comparison, the red traces display the $\mathrm{d}I/\mathrm{d}V$ curve for that particular device obtained at 20 K before deposition. The observed resonance peaks are a signature of one or more transport channels present in the molecular junction. As these resonances are only present after the deposition of molecules, they are attributed to the presence of the BPC molecule. In general, the position of these resonances reflects the electronic structure of the junction. These resonances are located at similar bias voltages, highlighted by the grey-shaded regions, which confirms the robustness and reproducibility of the BPC molecular junctions. We note, however, that the resonances exhibit different amplitudes, which may be attributed to local variations in the junction conformation.

Finally, we also note that for molecule C, the mechanical anchoring to the substrate is stable, even though the electronic transport is not. In the Supplementary Information, using a statistical cross-correlation analysis, we show that similar electronic features are observed across multiple devices, which demonstrates that, indeed, the anchoring to the substrate provides sufficient mechanical stability. However, owing to the smaller π–π overlap

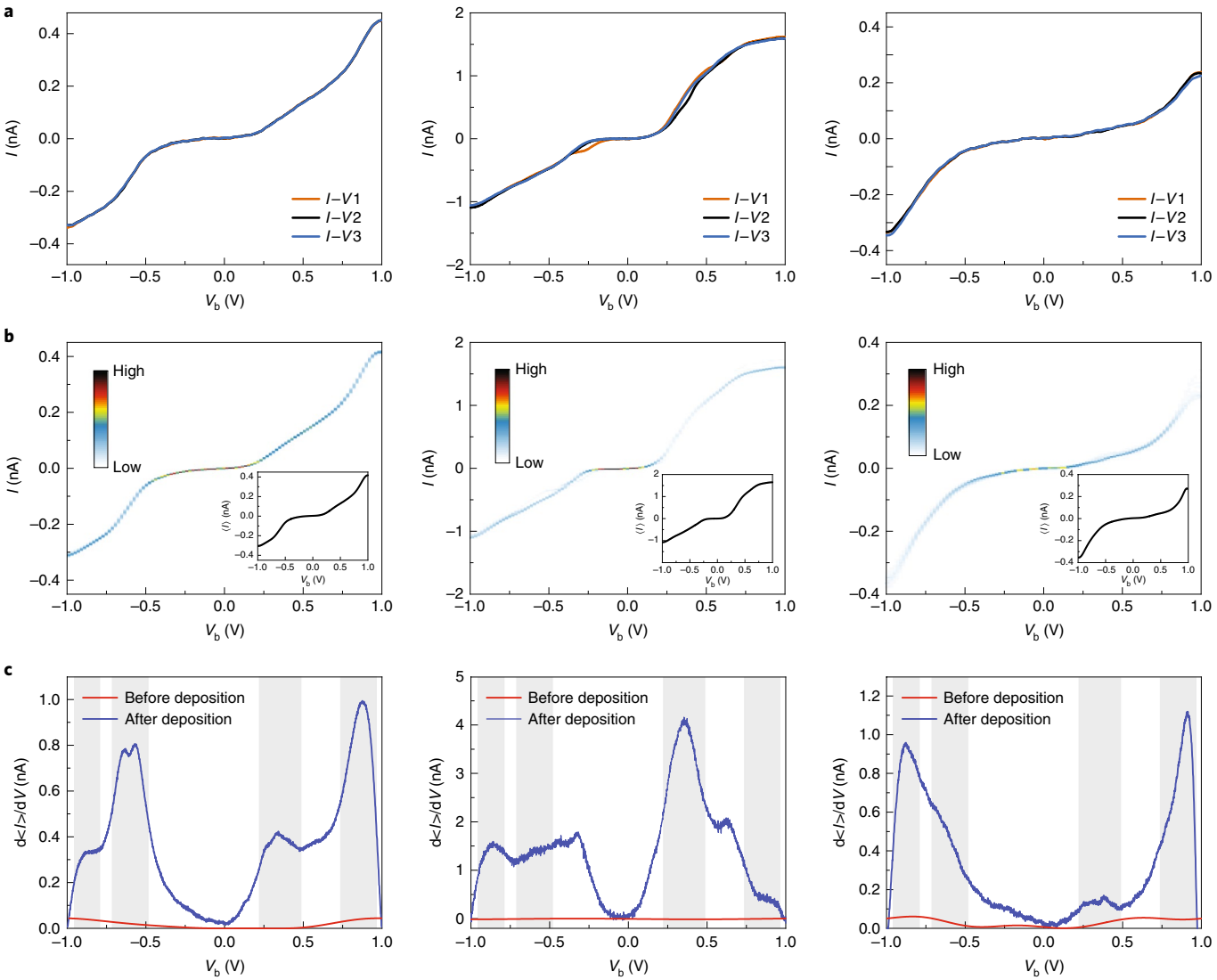

Fig. 2 | Electrical characterization of devices A (left), B (middle) and C (right) at 20 K exposed to the molecule BPC. a, Three individual *I*–*V* curves recorded for each device. **b**, Density plots of *I*–*V* curves. Insets: average *I*–*V* curves ⟨*I*⟩. **c**, d⟨*I*⟩/d*V* curves obtained before (red) and after (blue) deposition. The resonances observed after deposition correspond to the electronic energy levels of the molecular junction. The grey regions highlight the different resonances.

between the head groups compared to the BPC molecule, the electronic stability is limited.

Junction electronic robustness at different temperatures

We further investigated the junction stability by characterizing the devices in a large range of temperature that extended from 20 K to 300K. Figure 3a shows the density plot obtained from 100 *I*–*V* curves measured at three selected temperatures (20 K, 150 K and 300 K) for device A, with ⟨*I*⟩ shown in the insets. From the density plots, a high similarity between successive *I*–*V* curves is observed at all the temperatures. This behaviour highlights the high electronic and mechanical stability of the devices, in stark contrast to the behaviour of junctions based on molecule C (Fig. 1d). A similar observation can also be made from Fig. 3b. Here, the plot shows the evolution of d⟨*I*⟩/d*V* with temperature. The resonance positions remain fairly similar throughout the entire range, whereas the peak amplitudes steadily decay with increasing temperature.

Figure 3c presents the evolution of ⟨*I*⟩ as a function of temperature, plotted in a logarithmic scale. The plot shows that the current remains fairly constant over the entire temperature range for various bias voltage values, in particular in the high-temperature region between 150 K and 300 K. This observation suggests that the charge transport through these graphene–molecule–graphene junctions remains coherent up to 300 K. This appealing effect is in contrast with studies performed in systems in which electrons are transported incoherently through the device. In such cases, a strong reduction in current was observed for decreasing temperatures, which corresponded to activation energies in the 10–100 meV range[20–25]. Interestingly, the current through our device even increased slightly with decreasing temperature. This effect may be related to minor rearrangements of the molecules in the junction, which may also be the cause for the small jump in current measured at around 120 K. The temperature dependence of the empty graphene gaps was also investigated (Supplementary Information gives more details), but no significant effect of the temperature was observed, in agreement with a previous study[9]. Finally, Fig. 3d presents the evolution of the *I*–*V* curves over time at room temperature. No significant fluctuations were observed at bias values up to 1.0 V, which highlights the very high stability of the molecular junctions.

To investigate charge transport through these graphene–molecule–graphene junctions, we calculated the transmission probability *T*(*E*) of electrons with energy *E* that pass through the molecules

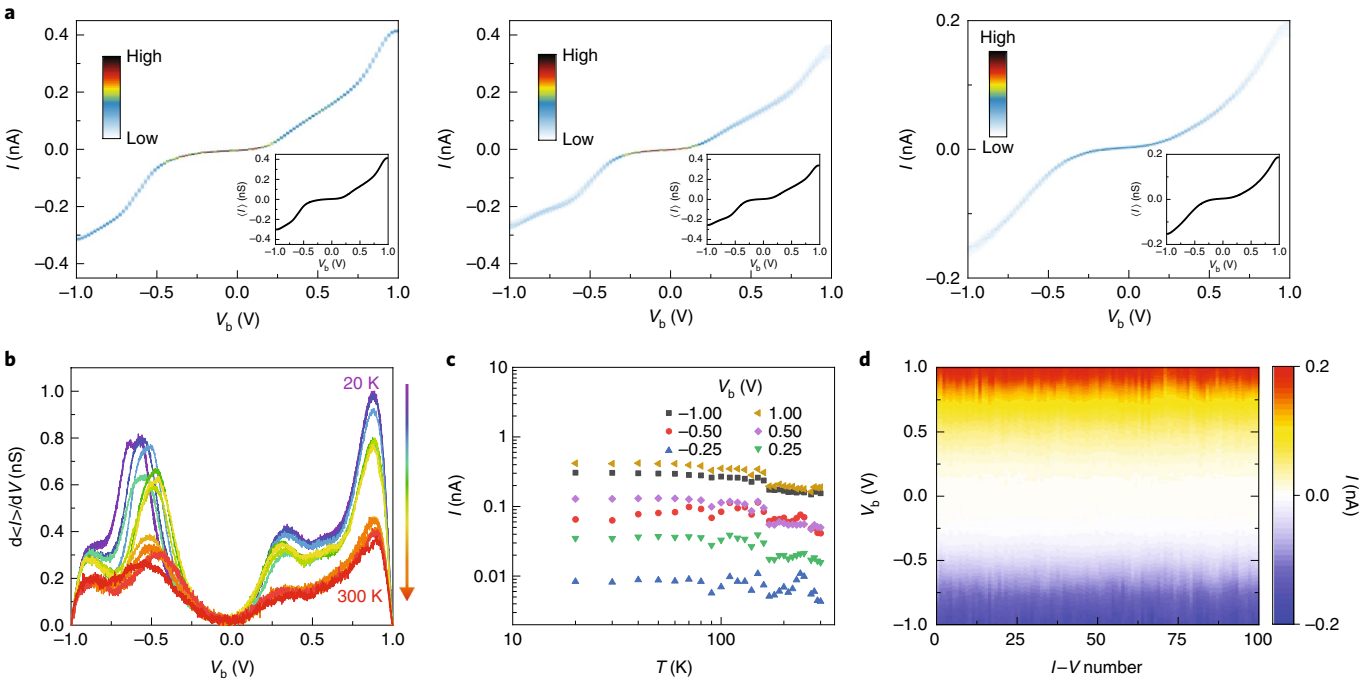

Fig. 3 | Transport measurements through a BPC molecular junction (device A) at different temperatures. a, Density plots constructed from 100 *I*–*V* curves for the three temperatures 20 K (left), 150 K (middle) and 300 K (right). **b**, Differential conductance $d\langle I\rangle/dV$ of the device shown in **a** plotted for increasing temperatures. **c**, Evolution of the absolute value of $\langle I\rangle$ as a function of the temperature plotted for different bias values in a log–log scale. **d**, Evolution over time of the *I*–*V* curves measured at 300 K.

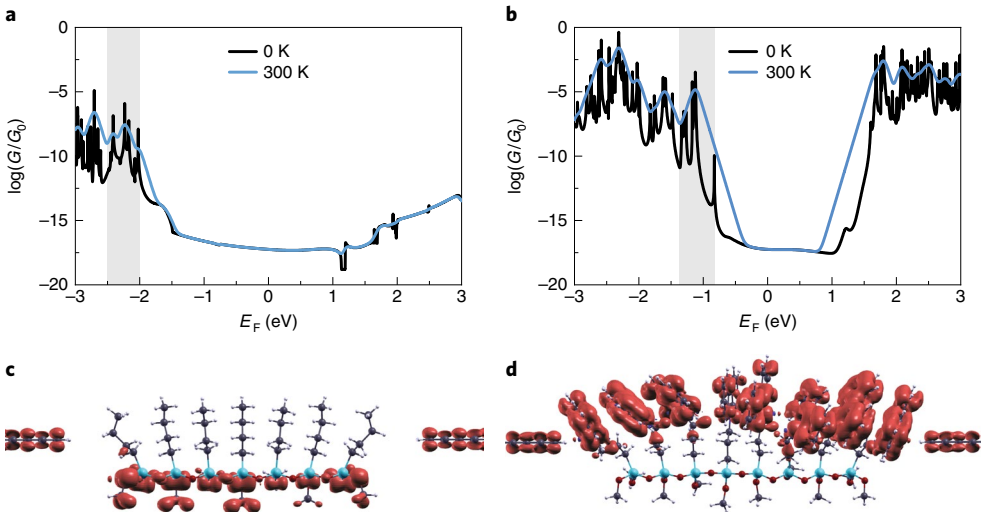

Fig. 4 | Transport through graphene–molecule–graphene junctions that containing the M and BPC molecule. a,**b**, Computed conductance for different values of E_F at $T = 0$ and 300 K for molecule M and molecule BPC, respectively. The grey-shaded areas correspond to the energy range used to compute the local density of states shown in **c** and **d**. Note that E_F is the Fermi energy of the junction relative to the DFT-predicted E_F and may be different from the experiments. **c**,**d**, Local density of states of the resonances closest to the Fermi energy of the electrodes for molecule M and BPC, respectively.

from one graphene electrode to another (Methods). We obtained the material-specific mean-field Hamiltonian from the SIESTA implementation of DFT[26] combined with the Gollum implementation of the non-equilibrium Green's function method to calculate $T(E)$ (ref. [27]) (Methods). The conductance G was calculated for different Fermi energies (E_F) and temperatures using the Landauer formula, $G = G_0 \int dE T(E)(-df/dE)$ where $G_0 = 2e^2/h$ is the conductance quantum, $f = (1 + \exp((E - E_F)/k_BT))^{-1}$ is the Fermi–Dirac distribution function, T is the temperature and $k_B = 8.6 \times 10^{-5}$ eV K^{-1} is Boltzmann's constant.

Figure 4a,b shows the computed conductance (G/G_0) for the reference molecule M and molecule BPC for a particular junction geometry. Transmissions were also calculated for other geometries (Supplementary Section II). The calculations show that the transmission through the reference molecules is systematically lower than that for the BPC molecule, regardless of the choice of the Fermi energy. This observation also holds for other junction configurations (Supplementary Section II). The drastically lower conductance is attributed to the gap between the highest occupied molecular orbital and the lowest unoccupied molecular orbital of

the graphene–molecule–graphene junction being larger for reference molecule M. We investigated the nature of the transport channels that dominate transport for both molecules; Fig. 4c,d displays the local density of states obtained in the energy window, highlighted in grey, that corresponds to the resonance closest to E_F. For the BPC molecule, the wavefunction extended over the biphenyl N-carbazole groups. For the reference molecule, however, no delocalized orbitals were formed and transport occurred via the poorly conducting silane groups. These calculations demonstrate the crucial role of π–π-stacked head groups in the transport, and rationalize the large difference in current observed experimentally for the two molecules.

We report here graphene-based molecular devices that are electronically and mechanically stable over a large temperature range. This was achieved by decoupling the mechanical anchoring from the electronic pathways by combining a covalent binding of the molecules to the substrate and large π-conjugated head groups. The junctions were reproducible over several devices and operated from 20 K up to room temperature. Our approach represents a simple but powerful strategy for the future integration of molecule-based functions into stable and controllable nanoelectronic devices.

Online content

Any methods, additional references, Nature Research reporting summaries, source data, statements of code and data availability and associated accession codes are available at https://doi.org/10.1038/s41565-019-0533-8.

Received: 31 January 2019; Accepted: 22 July 2019;
Published online: 16 September 2019

References

1. van der Molen, S. J. et al. Visions for a molecular future. *Nat. Nanotechnol.* **8**, 385–389 (2013).
2. Aradhya, S. V. & Venkataraman, L. Single-molecule junctions beyond electronic transport. *Nat. Nanotechnol.* **8**, 399–410 (2013).
3. Sadeghi, H., Sangtarash, S. & Lambert, C. Robust molecular anchoring to graphene electrodes. *Nano Lett.* **17**, 4611–4618 (2017).
4. Tao, N. Electron transport in molecular junctions. *Nat. Nanotechnol.* **1**, 173–181 (2006).
5. Lau, C. S. et al. Redox-dependent Franck–Condon blockade and avalanche transport in a graphene–fullerene single-molecule transistor. *Nano Lett.* **16**, 170–176 (2015).
6. Barreiro, A., van der Zant, H. S. & Vandersypen, L. M. Quantum dots at room temperature carved out from few-layer graphene. *Nano Lett.* **12**, 6096–6100 (2012).
7. Sadeghi, H. et al. Conductance enlargement in picoscale electroburnt graphene nanojunctions. *Proc. Natl Acad. Sci. USA* **112**, 2658–2663 (2015).
8. Gehring, P. et al. Quantum interference in graphene nanoconstrictions. *Nano Lett.* **16**, 4210–4216 (2016).
9. Prins, F. et al. Room-temperature gating of molecular junctions using few-layer graphene nanogap electrodes. *Nano Lett.* **11**, 4607–4611 (2011).
10. Jia, C. et al. Covalently bonded single-molecule junctions with stable and reversible photoswitched conductivity. *Science* **352**, 1443–1445 (2016).
11. Su, T. A., Neupane, M., Steigerwald, M. L., Venkataraman, L. & Nuckolls, C. Chemical principles of single-molecule electronics. *Nat. Rev. Mater.* **1**, 16002 (2016).
12. Li, S. et al. The evolving quality of frictional contact with graphene. *Nature* **539**, 541–545 (2016).
13. Mol, J. A. et al. Graphene–porphyrin single-molecule transistors. *Nanoscale* **7**, 13181–13185 (2015).
14. Xu, Q. et al. Single electron transistor with single aromatic ring molecule covalently connected to graphene nanogaps. *Nano Lett.* **17**, 5335–5341 (2017).
15. Yao, J., Zhong, L., Natelson, D. & Tour, J. M. Silicon oxide: a non-innocent surface for molecular electronics and nanoelectronics studies. *J. Am. Chem. Soc.* **133**, 941–948 (2011).
16. Pósa, L. et al. Multiple physical time scales and dead time rule in few-nanometers sized graphene–SiO_x–graphene memristors. *Nano Lett.* **17**, 6783–6789 (2017).
17. Aswal, D., Lenfant, S., Guerin, D., Yakhmi, J. & Vuillaume, D. Self-assembled monolayers on silicon for molecular electronics. *Anal. Chem. Acta* **568**, 84–108 (2006).
18. DiBenedetto, S. A., Facchetti, A., Ratner, M. A. & Marks, T. J. Molecular self-assembled monolayers and multilayers for organic and unconventional inorganic thin-film transistor applications. *Adv. Mater.* **21**, 1407–1433 (2009).
19. Krasnoslobodtsev, A. V. & Smirnov, S. N. Effect of water on silanization of silica by trimethoxysilanes. *Langmuir* **18**, 3181–3184 (2002).
20. Hines, T. et al. Transition from tunneling to hopping in single molecular junctions by measuring length and temperature dependence. *J. Am. Chem. Soc.* **132**, 11658–11664 (2010).
21. Segal, D., Nitzan, A., Davis, W. B., Wasielewski, M. R. & Ratner, M. A. Electron transfer rates in bridged molecular systems 2. A steady-state analysis of coherent tunneling and thermal transitions. *J. Phys. Chem. B* **104**, 3817–3829 (2000).
22. Kim, H. & Segal, D. Controlling charge transport mechanisms in molecular junctions: distilling thermally induced hopping from coherent-resonant conduction. *J. Chem. Phys.* **146**, 164702 (2017).
23. Hihath, J. Charge transport in the inverted Marcus region. *Nat. Nanotechnol.* **13**, 276–277 (2018).
24. Yuan, L. et al. Transition from direct to inverted charge transport Marcus regions in molecular junctions via molecular orbital gating. *Nat. Nanotechnol.* **13**, 322–329 (2018).
25. Selzer, Y., Cabassi, M. A., Mayer, T. S. & Allara, D. L. Thermally activated conduction in molecular junctions. *J. Am. Chem. Soc.* **126**, 4052–4053 (2004).
26. Soler, J. M. et al. The SIESTA method for ab initio order-*N* materials simulation. *J. Phys. Condens. Matter* **14**, 2745 (2002).
27. Ferrer, J. et al. Gollum: a next-generation simulation tool for electron, thermal and spin transport. *New J. Phys.* **16**, 093029 (2014).

Acknowledgements

We thank C. Schönenberger for fruitful discussions. This work was partially supported by the European Commission FP7-ITN Molecular-scale Electronics: Concepts, Contacts and Stability (MOLESCO) grant (no. 606728) and the FET open project QuIET (no. 767187). This work was supported by UK Engineering and Physical Sciences Research Council Grant EP/M014452/1 and EP/N017188/1 and the European Research Council Advanced Grant (Mols@Mols). H.S. acknowledges the UK Research and Innovation for Future Leaders Fellowship no. MR/S015329/1 and the Leverhulme Trust for Leverhulme Early Career Fellowship no. ECF-2017-186. S.S. acknowledges the Leverhulme Trust for Early Career Fellowship no. ECF-2018-375. M.L.P. acknowledges the funding by the EMPAPOSTDOCS-II programme, which has received funding from the European Union's Horizon 2020 research and innovation programme under the Marie Skłodowska–Curie Grant Agreement no. 754364. O.B. acknowledges technical support from the Binning and Rohrer Nanotechnology Center (BRNC).

Author contributions

M.E.A. conducted the measurements and performed the data analysis. O.B. and M.E.A. fabricated the devices. X.L, S.-X.L., S.D. and S.Y. provided the molecules. S.S. and H.S. provided the theory and performed the DFT calculations. M.E.A., M.L.P., H.S., H.S.J.vdZ., C.L. and M.C. designed and supervised the study. M.E.A., M.L.P., S.S. and H.S. wrote the paper. M.E.A., M.L.P., S.S., H.S. and M.C. participated in the discussion of the data. All the authors discussed the results and commented on the manuscript.

Competing interests

The authors declare no competing interests.

Additional information

Supplementary information is available for this paper at https://doi.org/10.1038/s41565-019-0533-8.

Reprints and permissions information is available at www.nature.com/reprints.

Correspondence and requests for materials should be addressed to S.-X.L., H.S. or M.C.

Peer review information *Nature Nanotechnology* thanks Dirk Mayer and the other, anonymous, reviewer(s) for their contribution to the peer review of this work.

Publisher's note Springer Nature remains neutral with regard to jurisdictional claims in published maps and institutional affiliations.

Methods

Molecular synthesis. M and C molecules were purchased from Sigma-Aldrich. Details of the synthesis of the BPC molecule are presented in the Supplementary Section I.

Junction formation. The molecular junctions were formed as follows. First, nanogaps were created in the graphene devices using an electrical breakdown technique, as described in previous studies[9,28,29]. The graphene gaps were first characterized at room and low temperature, before deposition of the molecules. Only junctions with resistances higher than 1 GΩ and that showed no gate dependence were selected for further use. After characterization of the empty gaps, the devices were immersed for 20 h at 80° degrees in a solution that contained dry toluene and the molecules of interest (0.1 mM). The samples were then successively rinsed with dichloromethane, acetone and isopropanol. In the case of the BPC molecule, 46 gaps were formed by electrical breakdown. Of these, 29 were characterized at both low and room temperature. After deposition, 23 of these junctions were measured and 9 out of the 23 showed a signal after transfer.

Molecular dynamic. To understand how the 3-carbazolylpropyltrimethoxysilane molecules interact with graphene electrodes, molecular dynamic simulation was carried out using the ADF[30] reaxFF package. The VelocityVerlet and Berendsen molecular dynamics methods were used with 0.250 fs steps. The atomic positions belong to the SiO_2 substrate and the parts of the graphene electrodes far from the scattering region were constrained. The simulation was run for 150,000 molecular dynamics iterations. Snapshots of the atomic coordinates of the junctions were taken. These coordinates were used as the initial geometries of the device for the DFT calculations.

DFT calculation. The optimized geometry of each structure studied in this work was obtained self-consistently for forces smaller than 20meV $Å^{-1}$ using the SIESTA[26] implementation of the DFT with an energy cut-off of 250 Ry for the real-space grid and a double-ζ polarized basis set. Linear combination of atomic orbitals are employed in SIESTA to construct the valence states and norm-conserving pseudo potentials to account for the core electrons. We use the generalized gradient approximation of the exchange and correlation functional with the Perdew–Burke–Ernzerhof parameterization. The local density of states (LDOS), which is the DOS weighted by the amplitude of the corresponding wavefunctions at different points in space, were then obtained over a range of energies.

Transport. We obtained the ground state mean-field Hamiltonian and overlap matrix from the optimized geometries of the converged SIESTA DFT calculations. To calculate the phase-coherent, elastic scattering properties of each junction, these Hamiltonian (H) and overlap (S) matrices were combined with the Gollum[27] implementation of the non-equilibrium Green's function method. Each junction consists of left (source) and right (drain) graphene leads connected to the scattering region formed from 3-carbazolylpropyltrimethoxysilane molecules. The transmission coefficient $T(E)$ for electrons of energy E (that pass from the source to the drain) was calculated via the relation $T(E) = \mathrm{trace}(\Gamma_R(E)G^R(E)\Gamma_L G^{R^\dagger}(E))$ where $G^R = (ES - H - \Sigma_L - \Sigma_R)^{-1}$ is the retarded Green's function, $\Gamma_{L,R}(E) = i(\Sigma_{L,R}(E) - \Sigma_{L,R}^\dagger(E))$ describes the level broadening due to the coupling between the left (L) and right (R) electrodes and the central scattering region, and $\Sigma_{L,R}$ are the retarded self-energies. The electrical conductance was calculated using the Landauer formula $G = G_0 \int dE \cdot T(E)\left(\frac{-df(E)}{dE}\right)$.

Data availability

The data that support the plots within this paper and other findings of this study are available from the corresponding authors upon reasonable request. Measurements and analysis were performed in Origin and Matlab. All codes are available from the authors upon reasonable request.

References

28. Nef, C. et al. High-yield fabrication of nm-size gaps in monolayer CVD graphene. *Nanoscale* **6**, 7249–7254 (2014).
29. El Abbassi, M. et al. From electroburning to sublimation: substrate and environmental effects in the electrical breakdown process of monolayer graphene. *Nanoscale* **9**, 17312–17317 (2017).
30. Chenoweth, K., van Duin, A. C. T. & Goddard, W. A. Reaxff reactive force field for molecular dynamics simulations of hydrocarbon oxidation. *J. Phys. Chem. A* **112**, 1040–1053 (2008).